System Identification and Semiactive Control of a Squeeze-Mode Magnetorheological Damper

Chih-Jer Lin, *Member, IEEE*, Her-Terng Yau, *Member, IEEE*, Chun-Ying Lee, and Kai-Hung Tung

***Abstract*—The main goal of this investigation is to establish modeling of a squeeze-mode magnetorheological (MR) damper and to design a semiactive fuzzy controller for vibration reduction. To model the MR damper, the Bouc–Wen model has been used in many past studies. However, using the Bouc–Wen model to characterize the squeeze-mode MR damper needs a lookup table of system parameters for the application with various amplitudes and frequencies. Therefore, a biviscosity model is proposed to describe this squeeze-mode MR damper. In addition, genetic-algorithm-based optimization is used to evaluate the parameters of the system. To reduce the vibration of the structure, a semiactive fuzzy controller using the MR damper is presented for the structure vibration at various frequencies. To check the consistency of the proposed fuzzy controller, the real-time implementation validated the performance of the controller.**

***Index Terms*—Biviscosity model, Bouc–Wen model, fuzzy control, genetic algorithm (GA), magnetorheological (MR) damper, squeeze mode.**

I. Introduction

VIBRATION control of large-scale civil infrastructure is of utmost importance for human society and our daily lives. Because magnetorheological (MR) dampers have the capability of varying the amount of damping, they have been applied to protect skyscrapers and high-speed railways from earthquake hazard via base isolation or reduced structural vibrations caused by seismic motions. Magnetorheological fluid (MRF) technology has already been successfully employed in applications of automotive semiactive suspension and structural vibration reduction. The rheological behavior of MRF shows that the external magnetic field determines the relationship between the shear stress and the shear rate, and makes it become a Newtonian fluid or a Bingham fluid. When no magnetic field is present, MRF is like a Newtonian fluid and very similar to the pattern of the carrier fluids, except that the metal powder content makes the liquid slightly "thicker" [1], [2]. When a magnetic field is present, it shows the characteristics of a Bingham fluid, with the magnetic field causing some resistance at zero shear rate. Under this condition, the resistance force causes a plastic deformation and the yield stress is a function of the magnetic field strength. The magnetic field results in viscosity changes, and the MRF can be controlled to become a free flowing liquid or a semisolid condition.

According to the fluid flow and the rheological stress, MRF operations can be separated into three different modes: the valve mode, the shear mode, and the squeeze mode [1]. The first operational mode is the valve mode. This mode is usually used in dampers and shock absorbers [2]–[5]. For example, heavy-duty vehicle seat suspension uses a valve-mode MR damper as a secondary suspension element to improve the antivibration effect [6]. The valve-mode MR damper consists of a controllable fluid valve and a hydraulic cylinder filled with MR fluids, which are made of base fluids, additives, and a suspension of micrometer-sized, magnetically polarizable metal particles. A magnetic coil is integrated into the piston of the damper to generate a magnetic field. When a magnetic field is applied, each metal particle becomes a dipole, and some chains are formed by the metal particles due to the effect of the magnetic field. Because the chains cause a mechanical resistance to the fluid flow, the viscosity of the fluid is increased by increasing the magnetic field. The MR effect is reversible, and the mechanical resistance can be controlled by the magnetic field strength. The yield stress capability also depends on the magnetization characteristics of the particles. Since 2002, the valve-mode dampers have been manufactured by GM/Delphi for vehicle suspension. Other possible applications using the valve-mode operation are vibration dampers, active engine mounts, and seismic dampers for civil industry [7], [8].

The second operational mode is the shear mode, also called the direct shear mode, which is used in the application of brakes and clutches [9]. For example, an MR brake consists of a shaft, bearings, sealing devices, a housing with a coil, an interface disc, and MRF. The total shear force is separated into a viscous component and a magnetic-field-dependent component. The MRF brake is manufactured as a controllable resistance element for programmable aerobic exercise equipment. The valve and the direct-shear modes have been studied in detail, and some products using these two modes have already been manufactured and sold in many applications of structural vibration absorbers and automotive suspension. However, for some applications which need a higher ratio of the MRF effect, the capabilities of the valve mode and the direct-shear mode are challenging. Some researchers have reported that the other operation mode can

Manuscript received December 10, 2012; revised May 22, 2013; accepted August 17, 2013. Date of publication September 10, 2013; date of current version December 11, 2013. Recommended by Guest Editor O. Sawodny. This work was supported by the National Science Council of Taiwan under Grant NSC 101-2221-E-027-029.

C.-J. Lin and K.-H. Tung are with the Graduate Institute of Automation and Technology, National Taipei University of Technology, Taipei 10608, Taiwan (e-mail: cjlin@ntut.edu.tw; les322232@hotmail.com).

H.-T. Yau is with the Department of Electrical Engineering, National Chin-Yi University of Technology, Taichung 41170, Taiwan (e-mail: htyau@ncut.edu.tw).

C.-Y. Lee is with the Department of Mechanical Engineering, National Taipei University of Technology, Taipei 10608, Taiwan (e-mail: leech@ntut.edu.tw).

Color versions of one or more of the figures in this paper are available online at http://ieeexplore.ieee.org.

Digital Object Identifier 10.1109/TMECH.2013.2279852

achieve a higher MRF effect than either the valve or the shear mode. For small-amplitude motions, the *squeeze-mode* operation seems to offer very large forces which can be controlled by the MRF effect. Zhang implemented some experiments and evaluated theoretically to confirm whether yield stress ten times as large as that with either the valve mode or the shear mode could be achieved [10]. For the MR operations in squeeze mode, there is no particle saturation at low-compression stress stage; thus, the yield stress increases linearly with increasing magnetic field strength. For the squeeze mode, the distance of particles becomes shorter as the pressure load is increasing and the interaction of dipoles becomes stronger. However, for the valve mode or shear mode, the distance of particles does not vary as the pressure is applied. Therefore, the yield stress for the squeeze mode increases more than the other two modes, because the formed chain structure is difficult to be broken. As the compression stress is higher, the squeeze-strengthen effect is more obvious. This is called the squeeze-strengthening effect [10]. The stronger MRF effect of squeeze mode makes MRF technology more attractive for the next generation of structural vibration reduction.

MR dampers' inherently hysteretic nonlinear dynamics make the control of their practical use significantly difficult. Therefore, the modeling of MR damping is very important for its applications. To characterize the performance of MR dampers, several works have been performed to model their nonlinear behavior [11]. These investigations include the phenomenological model based on a modified Bouc–Wen model to describe the hysteretic behavior of the MR damper proposed by Spencer *et al*. [12], the nonlinear viscoelastic-plastic model proposed in [13] and [14], the neural network model proposed by Chang and Roschke [15], [16], the fuzzy model [17], the polynomial model [18], the NARX model [19], the extended Bouc–Wen model [20]–[23], and other approaches [24], [25]. However, the extended Bouc–Wen model involves many parameters to capture both the force–displacement and force–velocity hysteresis loops accurately. Additionally, the MR damper in the squeeze mode is a highly nonlinear device which has not been studied as thoroughly as those in the valve mode and the shear mode.

Since buildings are getting much taller, it is very difficult to obtain exact mathematical equations to describe the dynamics, especially for those structures which have a semiactive MR damper or dynamic vibration absorbers. Therefore, semiactive or active vibration control of structure systems using fuzzy set theory has been studied in the past few decades. The fuzzy set theory was proposed by Zadeh in 1965 [26], and Mamdani successfully applied the "IF–THEN" rule to the automatic control of a steam generator based on the fuzzy linguistic approach in 1974 [27]. In civil engineering, the fuzzy set theory has been applied by many investigations [28]–[30]. The success of the fuzzy controller depends on the correctness of the fuzzy rules which are usually determined by the experimental results of expert experience systems. However, the actual experiments for a novel complicated mechatronic system are sometimes costly in terms of both time and money. To simplify the problem, an optimization problem to determine the fuzzy rules is studied via the simulation of the estimated model.

TABLE I
SPECIFICATION OF MRF-122EG (MADE BY LORD) [32]

Appearance	Dark Gray Liquid
Viscosity, Pa-s @ 40°C (104°F) Calculated as slope 500-800 sec^{-1}	0.042 ± 0.020
Density, g/cm^3 (lb/gal)	2.28 (2.48)
Solids Content by Weight, %	72
Flash Point, °C (°F)	>150 (>302)
Operating Temperature, °C (°F)	-40 to +130 (-40 to +266)

In this study, a squeeze-mode MR damper is fabricated and studied. First, a modified Bouc–Wen model is used to capture the force–displacement relation of this damper. To identify the system parameters, a genetic algorithm (GA)-based optimization approach is studied [31]. GAs are stochastic optimization techniques based on the idea of natural evolution. GA, developed by Holland [15], is a search process based on natural selection. GAs belong to the larger class of evolutionary algorithms, which generate solutions to optimization problems using techniques inspired by natural evolution, such as inheritance, mutation, selection, and crossover. The optimization based on GA is very similar to nature, where the information is coded on the DNA. GAs are based on the ideas associated with the natural evolution of species, where the "fittest" organisms in a population survive and pass (through their genes) to the next generation, and so forth. The system parameters are coded with binary codes of N bits and they are performed via the genetic operations, which are inheritance, mutation, selection, and crossover, to obtain the optimal solution. However, based on the system identification results using the Bouc–Wen model for this squeeze-mode damper, the system parameters vary with respect to the different frequencies and amplitudes of the vibration input. Therefore, a modified biviscosity model is proposed to improve this drawback of the modeling.

II. SYSTEM DESCRIPTION AND MODELING OF THE MR DAMPER

A. System Description and Experimental Setup

For small motions of the damper, the squeeze-mode MRF offers the possibility of very large forces which can be controlled by the MRF effect. Additionally, the yield stress produced in the squeeze mode would be ten times as large as that in either valve mode or shear mode. To investigate the potential application of the squeeze-mode MR dampers in vibration control, an experimental apparatus is developed to study the relationship between the force and the displacement.

MR fluid actuated in squeeze mode is not a fully enclosed design. The fluid gap size is decreased and the available volume for the fluid is reduced from its original state as the MRF is compressed. In this study, the MR fluid is MRF-122EG, which is manufactured by LORD, and the datasheet is shown in Table I [32]. Fig. 1 shows the schematic diagram for measuring the MRF's characteristics in squeeze mode, where it is contained in an aluminum alloy vessel, and the base is an iron column wound with a copper coil. The MRF is compressed between two parallel plates. Therefore, it is mainly operated in squeeze mode. The

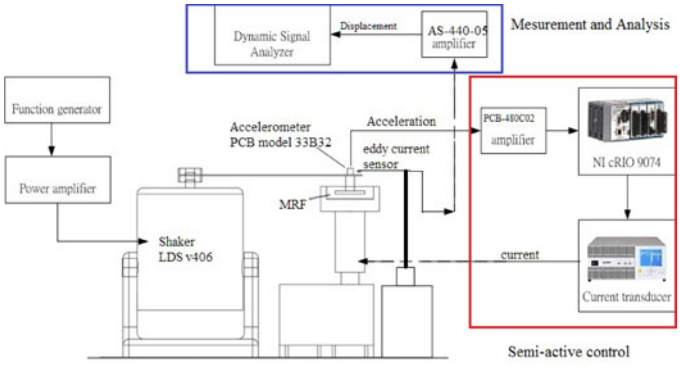

Fig. 1. Experimental apparatus for measuring the MR damper and implementing the semiactive control.

TABLE II
SPECIFICATION OF THE EDDY CURRENT DISPLACEMENT SENSORY SYSTEM

Amplifier Unit	AS-440-05
Sensor head	AH-416
Shape and dimension	
Measurement range	0~5 mm
Output voltage	0~5 V
Impedance	100Ω
Resolution	0.1% of FS
Linearity	± 1% of FS
Response	3.3kHz (-3dB)
Supply voltage	AC100/200V ± 15% 50/60Hz

upper squeezing plate is carried by the shaker, which produces the external vibration to test the characteristics of the MRF. The bottom of the iron column is connected to a load cell to measure the variation of the axial force during the experiments. An eddy current displacement sensory system (sensor: AH-416, amplifier: AS-440-05, made by KEYENCE) is equipped above the upper squeezing plate to measure its displacement which is produced by the shaker. The specification of this eddy current displacement sensory system is shown in Table II. Additionally, the experimental displacement and force signals are captured and analyzed using a dynamic signal analyzer (HP 35665A), which is also used to analyze the frequency response of the MRF damper in the later studies. The HP Analyzer is a two channel fast Fourier transformation (FFT) spectrum/network analyzer with a frequency range from near dc to just over 100 kHz. To measure the characteristics of squeeze-mode MRF via experiments, the oversized vessel (diameter of 80 mm) cooperates with the undersized piston (diameter of 50 mm), which allows the fluid to be expelled through the circumference of the piston. A coil electromagnet is used to generate a magnetic field by using a current supply. The steel coil magnet is joined with the bottom of the vessel, and the magnetic flux path passes through the MRF test vessel.

B. System Parameter Identification of the Bouc–Wen Model for the Squeeze-Mode Damper

For application of the MR damper in vibration control, Yao *et al.* adopted the Bouc–Wen model [20]. Therefore, in this

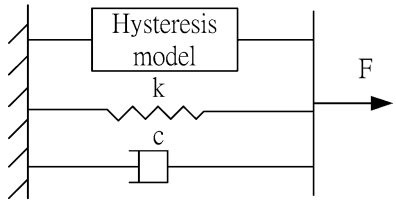

Fig. 2. Schematic diagram of the MR damper with nonlinear hysteresis model (viscous damping coefficient: c, stiffness coefficient: k, damping force: F).

study, the Bouc–Wen model is adopted to describe the dynamics of squeeze-mode MRF. The schematic diagram is shown in Fig. 2, and the force in the damper system is given by

$$F = c\dot{x} + kx + Az \tag{1}$$

where c is the viscous damping coefficient, k is the stiffness coefficient, and z is the hysteresis variable. A, c, k are all influenced by the input current to the coil. Moreover, the hysteresis variable is governed by

$$\dot{z} = \alpha\dot{x} - \beta\,|\dot{x}|\,z\,|z|^{n-1} - \gamma\dot{x}\,|z|^{n} \tag{2}$$

where α, β, γ parameters are related to the magnitude and shape of the hysteresis, and n is the smoothness coefficient which is used to control the smoothness transition from the elastic to the plastic region. To estimate the parameters of the model, a root mean square (RMS) error function is introduced as an objective function as follows:

$$J = \sqrt{\sum_{i=1}^{N} \frac{(F_e(i) - F_s(i))^2}{N}} \tag{3}$$

where $F_e(i)$ and $F_s(i)$ are the experimental damping force and the simulation damping force, which are computed via (1) and (2) using the same input signal in the actual experiment, and N is the number of the experimental data. Then, the procedures for identifying the system parameters are based on a GA optimization [31]. The optimization problem is described as follows:

$$\underset{c,k,A,\alpha,\beta,\gamma}{\text{Min}} \quad J(x,\dot{x},z) = \sqrt{\sum_{i=1}^{N} \frac{(F_e(i) - F_s(i))^2}{N}} \tag{4a}$$

subject to
equality constraints

$$\dot{z} = \alpha\,\dot{x} - \beta\,|\dot{x}|\,z\,|z|^{n-1} - \gamma\dot{x}\,|z|^{n} \tag{4b}$$

$$F_s = c\,\dot{x} + kx + Az \tag{4c}$$

and inequality constraints

$$0 \le c \le \bar{c}, 0 \le k \le \bar{k}, 0 \le A \le \bar{A}, 0 \le \alpha \le \bar{\alpha}, 0 \le \beta \le \bar{\beta},$$
$$0 \le \gamma \le \bar{\gamma}.$$

The above problem for identifying the parameters of the Bouc–Wen model is a nonlinear constrained optimization problem. It is difficult to perform this identification using MATLAB ID toolbox, because the problem is nonlinear. However, GA is a stochastic optimization technique based on the idea of natural evolution and it is suitable to obtain solutions for optimal

TABLE III
BOUC–WEN MODEL PARAMETERS WITH AMPLITUDE 0.05 mm AT 5 Hz

Current (A)	α	β	r	c	k	A	RMSE
0	0.675	50.46	0.063	0.124	3.1	0.087	0.050
1	0.863	51.64	0.096	0.170	3.399	0.185	0.065
2	0.970	40.74	0.050	0.237	3.403	0.891	0.054
3	0.896	43.36	0.071	0.271	4.092	0.920	0.115

search problems through application of the principles of evolutionary biology. In this study, a GA is adopted to identify the parameters $\{c, k, A, \alpha, \beta, \gamma\}$ of the Bouc–Wen model, which are constrained due to the physical limits. In this optimal problem, the objective function $J(x, \dot{x}, z)$ represents the RMSE between the experimental results and the simulation data. If the value of $J(x, \dot{x}, z)$ can be much smaller, then the estimated model will be more accurate. In this paper, the GA with binary code was applied to obtain the system parameters as the following steps. 1) Initial population generation: generates randomly a set of chromosomes for the parameters. 2) Fitness evaluation is to determine the fitness of the chromosomes to the objective function. 3) Selection operation is to determine pairs of chromosomes for mating. 4) Crossover operation is used for each pair of parents and it sets a parameter to be combined. 5) Mating operation is to combine the parameters by the crossover operator and swaps a certain number of parameters between each of the selected parents. 6) Mutation operation is to change randomly the value of a certain amount of parameters in the new offspring. Some of the parents and offspring are eliminated based on fitness value so as to keep the population size constant. Fitter chromosomes have higher probabilities of being selected. After several generations, the algorithm converges to the best chromosome, which hopefully represents the optimum or suboptimal solution to the problem [31].

To obtain the system parameters for this system, the excitation is applied to the system to measure the displacement and the damping force for the identification. The MR fluid actuated in squeeze mode is not a fully enclosed design. The gap between the upper squeezing plate and the vessel is 2 mm and the external excitation with amplitude of 0.05 mm at 5 Hz is applied to the upper plate. Therefore, the gap is decreased and the available volume for the fluid is reduced from its original state as the MRF is compressed. The estimated parameters are shown in Table III. Fig. 3 shows a comparison of the estimated responses and the corresponding experimental responses with amplitude of 0.05 mm at 5 Hz under various applied currents (0–3 A). From the simulation results, the estimated model can almost capture the properties of the MRF damper.

On one hand, Table III shows that the estimated parameters of the Bouc–Wen model vary for the various applied currents. On the other hand, the system parameters c, k, and A vary as the

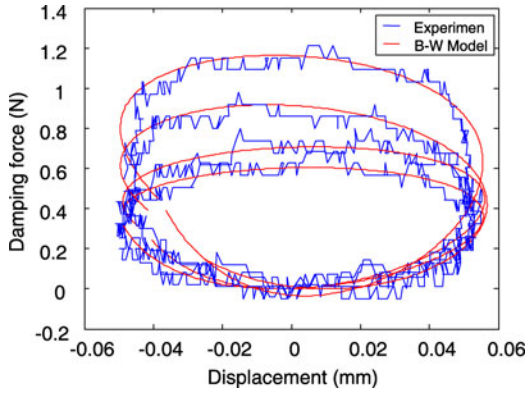

Fig. 3. Experimental response for the excitation with amplitude of 0.05 mm at 5 Hz in comparison with the simulation result using the Bouc–Wen model.

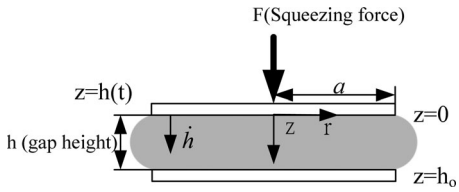

Fig. 4. Schematic diagram of a squeeze-mode MR damper with the gap height of h and the radius of a.

frequency or amplitude of the input excitation changes. Therefore, using the Bouc–Wen model to characterize the squeeze-mode MR damper needs a lookup table of system parameters for the application with various applied currents, excitation amplitudes, and frequencies. This situation may cause much difficulty if the vibration control is implemented using this model. Therefore, a biviscosity model is investigated in the following section to model the squeeze-mode MR damper.

III. MAIN RESULTS

A. Modeling of the Squeeze-Mode MR Damper Using the Biviscosity Model

The biviscosity model is proposed to describe the dynamic performance of an electrorheological fluid (ERF) in squeeze in a device where the fluid is sandwiched between two electrodes, one fixed and one moving in a direction normal to its own plane [33]. Therefore, this model is used to describe the squeeze-mode MR damper, because the working principle of the MRF is very similar to that of ERF, except for their different operations. ER uses the change of the electric field to tune the damping coefficient, while MR uses the change of the magnetic field. Fig. 4 shows that an MRF is contained in the space between two parallel circular plates of radius a.

The constitutive model chosen for the MRF is the well-known biviscosity mode and the yield stress of the fluid can be described as follows:

$$\tau(z) = \begin{cases} \eta_r \dfrac{du}{dz} & |\tau| < \tau_1 \\ \tau_0 + \eta \dfrac{du}{dz}, & |\tau| > \tau_1 \end{cases} \tag{5}$$

where u is the radial velocity of the fluid and $\gamma = \eta/\eta_r$. The relation between the constants τ_0 and τ_1 is as follows:

$$\tau_o = \tau_1(1-\gamma). \tag{6}$$

If the aspect ratio d/a is very small, where d is the average distance between two plates, the equation of motion is solved by applying the standard theory of lubrication. If the inertial effects are negligible, the equation of the shear stress is as follows:

$$\frac{\partial \tau}{\partial z} = \frac{dp}{dr} \tag{7}$$

where $\frac{dp}{dr}$ is the radial pressure gradient. If there are no-slip conditions on the plates, $u(h_0) = u(h(t)) = 0$ are given with the assumption that τ and u are continuous across the two yield surfaces in the fluid. Therefore, the two yield surfaces are expressed as follows:

$$z_1 = \frac{1}{2}\left(h_0 + h(t) + \frac{2\tau_1}{\frac{dp}{dr}}\right) \tag{8}$$

$$z_2 = \frac{1}{2}\left(h_0 + h(t) - \frac{2\tau_1}{\frac{dp}{dr}}\right). \tag{9}$$

If symmetry is considered in the flow, the mid-plane is as follows:

$$\bar{z} = \frac{1}{2}\left(h_0 + h(t)\right). \tag{10}$$

The vertical velocity of the movable plate can be obtained by the radial volumetric flow rate as follows:

$$\pi r^2 \dot{h}(t) = 2\pi r Q = 2\pi r \int_{z=h(t)}^{h_0} u dz \tag{11}$$

where $\dot{h}(t)$ is the vertical velocity of the movable plate. To make this equation more accessible, the dimensionless variables for the radial pressure gradient and radius are defined as follows:

$$G = -\left(\frac{h_0 + h(t)}{2\tau_1}\right)\frac{1}{r}\frac{dp}{dr} \tag{12}$$

and

$$S = \frac{\dot{h}(t)\eta r}{\left(h_0 + h(t)\right)^2 \tau_1}. \tag{13}$$

After the reductions, a relationship that determines G in terms of S and γ is described as follows:

$$G^3 - 3\left(S + \frac{1}{2}(1-\gamma)\right)G^2 + \frac{1}{2}(1-\gamma) = 0. \tag{14}$$

The main variable of interest is the average normal force over the bottom plate, which can be obtained by the following integration:

$$F = \int_{r=0}^{a} 2\pi r p(r) dr = -\pi \int_{r=0}^{a} r^2 \frac{dp}{dr} dr. \tag{15}$$

Then, expressing (15) in terms of the nondimensional variables defined by (12) and (13), it can be transferred as follows:

$$F = \frac{2\pi\tau_1 a^3}{h_0 - h(t)}\Psi(\chi) \tag{16}$$

where

$$\chi = S(a) = \frac{\dot{h}(t)\eta a}{\left(h_0 - h(t)\right)^2 \tau_1}$$

and

$$\Psi(\chi) = \frac{1}{\chi}\int_{S=0}^{\chi} S^2 G\, dS.$$

The yield stress of the MRF is assumed as follows:

$$\tau_1 = A_h H^b$$

where the magnetic field strength H is produced by the electromagnet, and A_h and b are the constants to be identified. The magnetic field strength H is obtained by the following equation:

$$H = \frac{NI}{2\pi R} \tag{17}$$

where I is the current passing through the electromagnet, R is the average radius of the electromagnet, and N is the number of turns.

In this biviscosity model, the system parameters η, γ, A_h, and b need to be identified using the optimization process. Therefore, the system identification of the biviscosity model for the squeeze-mode MR fluid is studied in the next section.

B. System Parameter Identification of the Biviscosity Model for the Squeeze-Mode Damper

The system parameter identification is considered as an optimization problem described as follows [24]:

$$\underset{\eta,\gamma,A_h,b}{\text{Min}} \quad J(x,\dot{x},z) = \sqrt{\sum_{i=1}^{N}\frac{(F_e(i) - F_s(i))^2}{N}} \tag{18}$$

subject to
equality constraints

$$F = \frac{2\pi\tau_1 a^3}{h_0 - h(t)}\Psi(\chi)$$

$$\chi = S(a) = \frac{\dot{h}(t)\eta a}{\left(h_0 - h(t)\right)^2 \tau_1}$$

$$\tau_1 = A_h H^b$$

and inequality constraints

$$0 \le \eta \le \bar{\eta}, 0 \le \gamma \le \bar{\gamma}, 0 \le A_h \le \bar{A}_h, 0 \le b \le \bar{b}.$$

Because the values for η, γ, A_h, and b are constant parameters to be identified, the procedures for identifying the system parameters are also based on the same GA optimization described in Section II. In the optimization, the inputs to the system are the measured displacement, the velocity, which is obtained by differentiating the displacement, and the measured force. The

TABLE IV
IDENTIFIED PARAMETERS OF THE BIVISCOSITY MODEL FOR THE MR DAMPER

η	γ	A_h	b
3.6877×10^{-6}	0.0793	5.2592×10^{-5}	1.9229

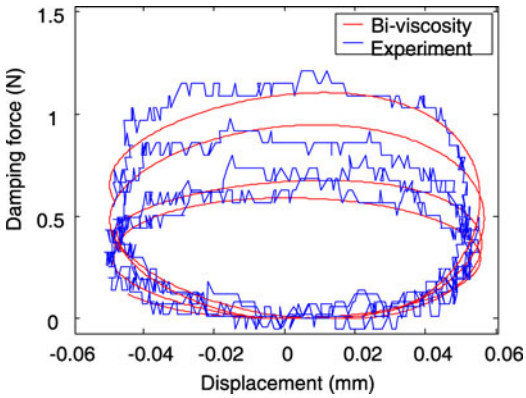

Fig. 5. Experimental response for the excitation with amplitude of 0.05 mm at 5 Hz in comparison with the simulation result using the biviscosity model.

TABLE V
COMPARISON OF MODELING ERRORS WITH AMPLITUDE OF 0.05 AND 0.1 mm USING THE BIVISCOSITY MODEL

Amplitude	0.05mm		0.1mm	
Frequency(Hz) / Current(A)	5	10	5	10
0	0.0469	0.0766	0.0754	0.0475
1	0.0543	0.0804	0.1057	0.0808
2	0.0737	0.068	0.0887	0.0838
3	0.0674	0.0827	0.0873	0.1072

estimated parameters for the biviscosity model at 5 Hz excitation with an amplitude of 0.05 mm are shown in Table IV, and a comparison of the experimental response and the simulation result is shown in Fig. 5. To verify the robustness of the biviscosity model, the same parameters η, γ, A_h, and b, obtained by the 5-Hz excitation, are applied to simulate the force–displacement relation with excitation at 10 Hz, and the RMS errors are shown in Table V. From a comparison of Tables III and V, the modeling error of the biviscosity model is better than that of the Bouc–Wen model except for the response of 2 A. However, the advantage of the biviscosity model is its robustness regarding the various inputs.

Using the same system parameters for biviscosity model obtained at 5 Hz to compare the experimental results with the simulation for excitations at 10 Hz, the results in Table V show that the modeling errors are in the permissible range. To verify the robustness of the biviscosity model with the various excitation amplitudes, the same system parameters obtained at 5 Hz are used to simulate the excitation at 5 Hz with amplitude of 0.1 mm, and Table V shows that the modeling errors are also in the permissible range. Therefore, the biviscosity model is used to investigate the design of the vibration control in this study.

IV. SEMIACTIVE CONTROL STRATEGY USING AN MR DAMPER FOR STRUCTURAL VIBRATION REDUCTION

A. Modeling of the Structure With the Squeeze-Mode MR Damper

Dyke *et al.* [34] have proposed a semiactive clipped-optimal control strategy for the MR damper, and a linear optimal controller was designed to adjust the command voltage. However, the command signal was discrete and set at either zero or the maximum level.

To study a semiactive fuzzy control strategy using the squeeze-mode MR damper, a model of a cantilever shaft with the MR damper is established. In this experiment, the structure consists of a shaft and a piston; the size of the shaft is 300 × 30 × 2 mm, the piston's diameter and thickness are 50 mm and 5 mm, and the shaft and the piston are made of aluminum alloy 6061. The squeeze-mode MR damper is the same as that described in Section II. The system identification problem is formulated as follows:

$$\underset{\text{fuzzy rules}}{\text{Min}}\ J(F_e, i) = \sqrt{\frac{1}{T}\int_0^T \ddot{x}^2 dt} \tag{19}$$

subject to

$$[M]\{\ddot{x}\} + [C]\{\dot{x}\} + [K]\{x\} = \{F^e\} + \{F^c\}$$

where $[M], [C], [K]$ are the mass, damping, and stiffness matrices of the structure, $\{x\}$ is the deflection of the structure, $\{F^e\}$ is the external excitation force, and $\{F^c\}$ is the controlled damping force produced by the MR damper. The damping force of the squeeze-mode MR damper is determined by the biviscosity model. To solve this optimization problem, the first step is to measure the frequency response of this structure via experiments. The second step is to obtain the structure model via simulation to match the actual model. The experiment was performed by applying random excitation to the structure via a shaker (LDS v406). Then, the HP 35665A was used to collect all of the frequency-domain data according to the shaker's acceleration and the deflection of the shaft. A PCB model-333B32 accelerometer and a PCB model-480C02 signal conditioner were used to measure the acceleration. The 333B32 accelerometer is capable of measuring frequencies from 0.5 to 3000 Hz with a 101.3-mV/g sensitivity. The acceleration range of the accelerometer is ±50 g peak. Additionally, the eddy current displacement sensory system AH-416 is used to measure the displacement. Fig. 6 shows the frequency-domain response of the cantilever shaft measured, and the first two modes' frequencies are approximately 11.5 and 96 Hz, as shown in Table VI.

Because the two modes are dominant for this structure, the deflection of the structure is approximated by the following equation:

$$\{x\} \approx \sum_{r=1}^{2} \Phi_r \eta_r(t) \approx [\Phi]\{\eta\} \tag{20}$$

where $[\Phi]$ is the modal matrix, and $\{\eta\}$ is the system response based on the coordinates of the mode. Consider that there are five nodes of the structure to be simulated as shown in Fig. 7;

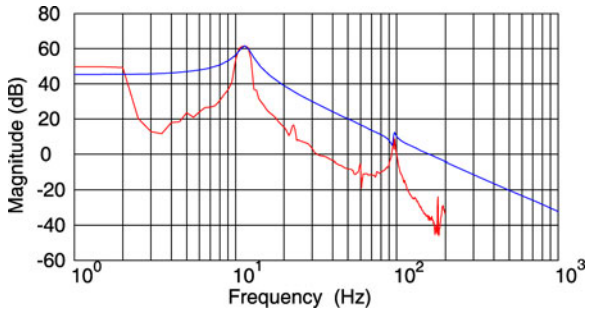

Fig. 6. Frequency response of the experimental and simulation results for the MRF damper system.

TABLE VI
COMPARISONS OF THE ACTUAL AND SIMULATION RESULTS

	1st Mode		2nd Mode	
	Frequency (Hz)	Amplitude (db)	Frequency (Hz)	Amplitude (db)
Experiment	11.5	61.46	96	9.435
Simulation	11.4	61.6	97	12.4

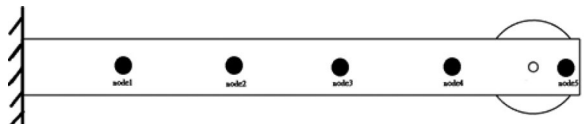

Fig. 7. Definition of nodes on the experimental structure.

the modal matrix is described as follows:

$$[\Phi]_{5\times 2} = [\,\Phi_1 \quad \Phi_2\,].$$

Therefore, the dynamics of the system are transferred as follows:

$$\bar{M}\{\ddot{\eta}\} + \bar{C}\{\dot{\eta}\} + \overline{K}\{\eta\} = \{\bar{F}^e\} + \{\bar{F}^c\} \tag{21}$$

where $\bar{M} = [\Phi]^T[M][\Phi] = I_{2\times 2}$, $\bar{C} = [\Phi]^T[C][\Phi] = [\text{diag}(2\xi\omega_n)]$, and $\bar{K} = [\Phi]^T[K][\Phi] = [\text{diag}(\omega_n^2)]$, $\{\bar{F}^e\} = \Phi^T\{F^e\}$ and $\{\bar{F}^c\} = \Phi^T\{F^c\}$. The damping ratio ξ for each mode can be obtained according to the frequency response of the structure. According to the frequency response, the damping ratio for each mode can be obtained using the half power bandwidth method [28]. This method is used to obtain an estimation of the damping of a structure. First, if the amplitude at the peak is P for the first mode, the method is to find the frequencies at which the amplitude of the transfer function is P_2 as follows:

$$P_2 = \frac{P}{\sqrt{2}} \approx 0.707P. \tag{22}$$

The frequencies ω_1 and ω_2 associated with the half power points on either side of the peak are obtained. Then the damping ratio ξ can be obtained using the formula as follows:

$$\xi = \frac{\omega_2 - \omega_1}{2\omega_n}. \tag{23}$$

The damping ratio and natural frequency for the first two modes are substituted into (21); therefore, the stiffness matrix and the damping matrix are $\bar{K} = 10^3 \cdot \begin{bmatrix} 0.1323 & 0 \\ 0 & 9.216 \end{bmatrix}$ and

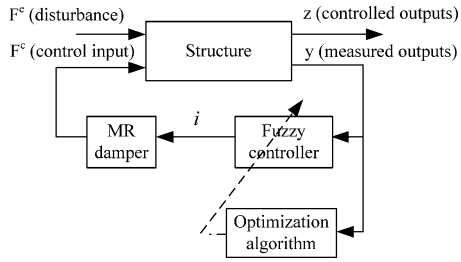

Fig. 8. Control diagram for the proposed semiactive fuzzy controller with optimal tuning.

$\overline{C} = \begin{bmatrix} 1.73 & 0 \\ 0 & 2.76 \end{bmatrix}$. On one hand, as an external excitation force $\{F^e\} = Ae^{j\omega t}$ is applied at Node 1, $\{\bar{F}^e\}$ at Node 1 can be obtained as follows:

$$\{\bar{F}^e\} = [\Phi]^T \cdot [1 \quad 0 \quad 0 \quad 0 \quad 0]^T Ae^{j\omega t} = \bar{H}_1 Ae^{j\omega t}.$$

On the other hand, the controlled damping force $\{\bar{F}^c\}$ at Node 5 can be given as

$$\{\bar{F}^c\} = [\Phi]^T \cdot [0 \quad 0 \quad 0 \quad 0 \quad 1]^T F_{MR} = \bar{H}_2 F_{MR}$$

where F_{MR} is the damping force, which can be obtained by the biviscosity model. Based on the experimental frequency response, the modal matrix can be obtained as follows:

$$[\Phi] = [\,\Phi_1 \quad \Phi_2\,] = \begin{bmatrix} 0.1727 & 2.5394 \\ 0.7728 & 5.2380 \\ 1.7753 & 5.9253 \\ 3.2263 & 3.9048 \\ 4.4086 & 2.5316 \end{bmatrix} \tag{24}$$

and

$$\bar{H}_1 = [\,75 \quad 0 \quad 0 \quad 0 \quad 0]^{\mathrm{T}}$$
$$\bar{H}_2 = [\,0 \quad 0 \quad 0 \quad 0 \quad 0.0012\,]^{\mathrm{T}}.$$

To verify the above model for this structure with the MR damper, the simulation is performed using the same excitation input and the biviscosity model with the zero control current; the frequency responses are shown in Fig. 6. Comparing the simulation results with the experimental results in Fig. 6, the frequency responses for the actual and simulation results are shown in Table VI. From the comparisons in Table VI, the simulated model almost matches the actual system in the first mode, and the modeling error in the second frequency is permissible in the frequency value. After the simulated model has been verified, the next step is to establish the fuzzy rule table based on the simulations for the various excitations.

B. Semiactive Fuzzy Controller Design via the Optimization Algorithm

For this semiactive vibration control task, the optimization for fuzzy controller is proposed. The main idea is that the fuzzy rule base is determined by the optimization algorithm as shown in Fig. 8. In this study, the design of the semiactive fuzzy controller selects the two response quantities to be used as input to

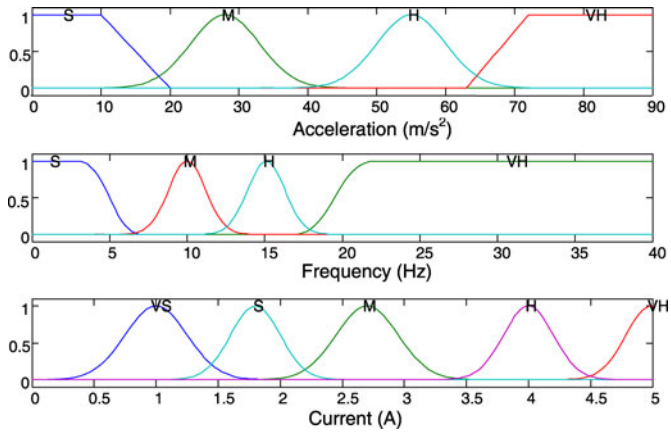

Fig. 9. Membership functions of the fuzzy controller.

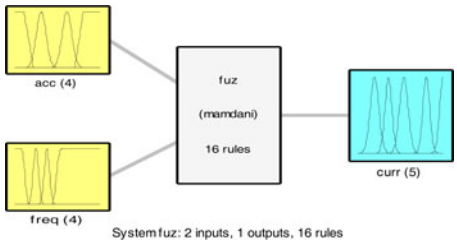

Fig. 10. Input–output relation of the fuzzy controller.

the fuzzy controller and one output from the controller to the MR damper. The two input variables are obtained via the measurement of the accelerometer equipped on the structure. The first input is the vibration frequency of the excitation, which can be obtained using the FFT from the acceleration signal, and the other input is the windowed root mean square value of the acceleration, which is obtained using the definition as follows:

$$\ddot{x}_{\text{eff}} = \sqrt{\frac{1}{T}\int_{t_s}^{t_e} \ddot{x}_5^2 dt}$$

where $\ddot{x}_5$ is the acceleration at the fifth node of the structure and T is the time interval of the windowed integration in the above equation. The windowed integration is used to integrate the signal over a sliding time window from t_s to t_e. In this windowed RMS integration, the beginning time is t_s and the terminal time is t_e, where $T = t_e - t_s$. Using this, windowed integration can effectively reject the noise of the accelerometer and reveal the quantity of the acceleration. For the proposed fuzzy controller, each one input is designed to have four membership functions to be used for the selected input variable, where one is the vibration frequency of the excitation and the other is the effective value of the acceleration. The output of the proposed fuzzy controller is the controlled current to the MR damper. The output is designed to have five membership functions as shown in Fig. 9, and the block diagram of the fuzzy controller is described in Fig. 10.

After determining the input and output of the semiactive fuzzy controller, how to obtain the fuzzy rule table is dominant to the performance. Because the model of the system has been established in the above section, the optimization of choosing the fuzzy rules can be obtained via the simulation results using

TABLE VII
LOOKUP TABLE FOR THE BEST CURRENT COMMAND OF THE MR DAMPER FOR THE VARIOUS EXCITATIONS

current (A) / Voltage (mV)	Applied frequency (Hz)			
	5	**10**	**15**	**20**
90	4	4	1	1
100	5	5	1	1
120	5	5	1	1

TABLE VIII
FUZZY RULE OF THE SEMIACTIVE CONTROLLER FOR THE MR DAMPER

MR damper current		Frequency of FFT (Hz)			
		S	M	H	VH
WRMS acc.	S	4	4	1	1
	M	5	5	1	1
	H	5	5	1	1

the specified excitation. Because the excitation amplitude is in proportion to the voltage applied to the shaker, the applied voltages with the various amplitudes and frequencies are applied to the shaker; then, the acceleration of the simulated model under the various inputted currents can be obtained. The windowed RMS values of the acceleration are obtained based on the input voltages to the shaker with amplitudes from 90 to 120 (mV). As a result, the fuzzy rules depend on the minimal windowed RMS value, and Table VII shows the lookup table for the best controlled current signals in the current range (0–5 A) for these tested excitations.

Higher applied voltage to the shaker causes greater vibration of the structure; therefore, the acceleration is in proportion to the voltage applied to the shaker. According to the lookup table in Table VII, the fuzzy rules can be intuitionally designed as Table VIII, where the first input is the windowed RMS value of the acceleration and the other is the vibration frequency of the excitation, which can be obtained using the FFT from the acceleration signal. For the two inputs, there are four membership functions, which include S (small), M (medium), H (high), and VH (very high), as shown in Fig. 9. For the output controlled current of the fuzzy controller, there are five membership functions as shown in Fig. 10, where a larger number means a larger current to the MR damper. Therefore, the architecture of the fuzzy controller can be implemented. To test the performance of the proposed fuzzy controller for the MR damper, the fuzzy rules are to implement for the fuzzy controller in real-time experiments in the following two case studies.

Fig. 1 shows the control block diagram for the real-time control architecture for this semiactive MR damping system, where the MR damper is self-designed as discussed in Section II and the coil electromagnet is used to generate a magnetic field to change the stiffness and damping coefficients of the MR damper. An NI CompactRIO 9074 with the 9234 and 9263 modules is used as the real-time embedded controller for the whole system. The NI 9234 has four analog input channels with a 24-bit Delta-Sigma ADC and it is used to capture the acceleration signal of the structure. The NI 9263 (Analog Output Module) is used to produce the control signal of the proposed fuzzy controller to

TABLE IX
VIBRATION REDUCTION OF THE PROPOSED CONTROLLER FOR THE EXPERIMENTAL STUDIES

Frequency	Reduction of amplitude
5Hz	2.83 %
10Hz	22.35%
15Hz	24.29%
20Hz	26.92 %

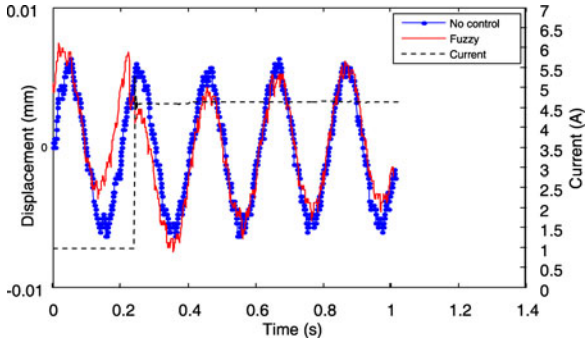

Fig. 11. Vibration response for the open-loop system and the system using the proposed controller for the excitation at 5 Hz.

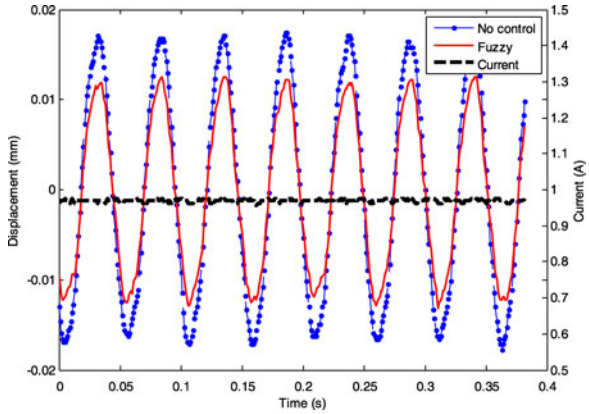

Fig. 12. Vibration response for the open-loop system and the system using the proposed controller for the excitation at 20 Hz.

TABLE X
PROPOSED RULE TABLE FOR THE FUZZY CONTROL AT LOW FREQUENCY

Current self-tune	$\dot{z} < 0$	$\dot{z} > 0$
$\ddot{z} < 0$	increase	decrease
$\ddot{z} > 0$	decrease	increase

the current supply (NF-BP4610). Since cRIO is made by National Instruments, the real-time controller can be programmed with LabVIEW (VI code), C, C++, or Java. However, LabVIEW must be used to program the embedded FPGA. In this study, a real-time control code embedded in cRIO 9074 is developed for the real-time implementation. Additionally, an eddy current displacement sensory system (sensor: AH-416, amplifier: AS-440-05, made by KEYNCE) is equipped above the upper plane of the structure to measure its displacement for comparisons. This coil electromagnet is actuated by a current supply (NF-BP4610). The top of the moving piston is equipped with an accelerometer (PCB model 333B32), which is incorporated with the PCB model-480C02 signal conditioner to measure acceleration.

Case I: The excitation signals with frequencies of 5, 10, 15, and 20 Hz are input to the shaker to make the structure vibrate. Table IX summarizes the performance of the semiactive fuzzy controller for excitation at the frequencies of 5–20 Hz. Figs. 11 and 12 show the comparisons between the open-loop system and the proposed controller at frequency of 5 and 20 Hz. Fig. 11 shows that the performance at 5 Hz is very poor, but the performance at 20 Hz is very well. Except for 5 Hz, the proposed fuzzy controller has a 22∼27% reduction in amplitude. To deal the worse performance at 5 Hz, the proposed fuzzy controller is amended and a self-tuning strategy is discussed in Case II.

Case II: In Case I, Fig. 11 shows that the performance at 5 Hz is very poor. Why the controller at 5 Hz has such poor performance could be ascribed to two reasons. One is because the acceleration at 5 Hz is too small to make the accelerometer sensitive enough. The other is that the semiactive control with the constant current cannot make the MRF provide the sufficient damping force for the vibration at low frequency and small displacement. Therefore, we introduce a novel self-tuning active control law for this MRF damper as the excitation's frequency is low. The idea of the proposed active control is inspired by the literature proposed by Dixon in 1999 [35].

According to the direction of the velocity and acceleration of the piston, Table X shows the self-tuning rule table for the active control law to determine the control current of MRF. First, consider the case with the positive velocity of piston. If the velocity of the piston is positive and the acceleration is negative, then the control current should be decreased to make the MRF reduce the damping force and let the structure go back to the neutral position. In the other case, if the velocity of the piston is positive and the acceleration is positive, then the control current should be increased to make MRF provide more damping force. Similarly, the other half control rules with the negative velocity of the piston can be derived as shown in Table X.

To verify whether the proposed controller can handle excitation at low frequency, the proposed self-tuning algorithm is used for the fuzzy control and Fig. 13 shows the comparisons between the response without control and with the proposed self-tuning + fuzzy controller. Fig. 14 shows the control current produced by the fuzzy controller. Resulting from Fig. 13, the proposed controller has a better vibration reduction (13.4%) than the one of the fuzzy control in Case I (2.83%). Therefore, the self-tuning method shows the improvement for small amplitudes at low frequency.

To verify whether the proposed controller can handle excitation of varying frequencies, two excitation signals are inputted to the system. The first signal with a frequency of 10 Hz is applied in the interval of $t = 0 \sim 4$ (s); then, the second signal at a frequency of 20 Hz is applied after $t = 4$ (s). Table XI summarizes the performance for vibration suppression for the excitation with various frequencies. The proposed self-tuning + Fuzzy controller has the better performance than the Fuzzy controller.

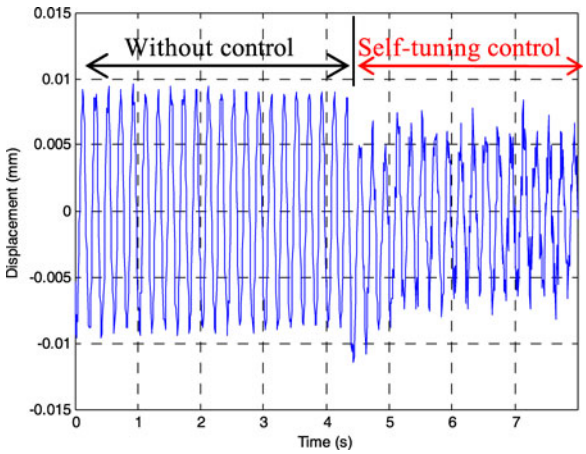

Fig. 13. Time response for the open-loop system and the self-tuning + fuzzy controller with the excitation at 5 Hz.

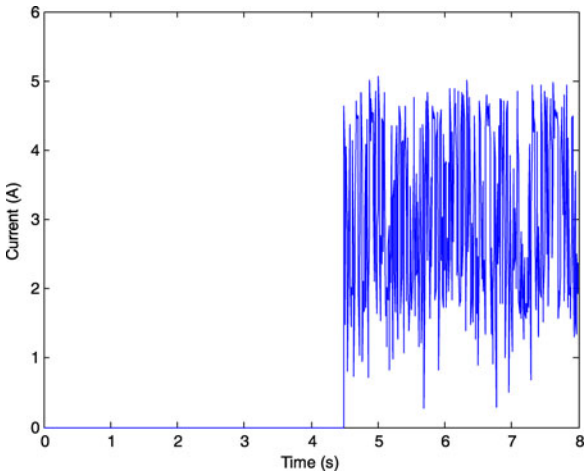

Fig. 14. Control current for the open-loop system and the self-tuning + fuzzy controller with the excitation at 5 Hz.

TABLE XI
VIBRATION REDUCTION OF THE PROPOSED CONTROLLER FOR THE PROPOSED METHODS AS THE EXCITATION'S FREQUENCY IS CHANGED FROM 10 TO 20 Hz

	5Hz→10Hz → 20Hz		
	5Hz	10Hz	20 Hz
self-tuning + Fuzzy	13.4 %	26.39%	27.99%
Fuzzy	2.83 %	20.13%	27.87%

The proposed controller has 26.39% and 27.99% reduction in amplitude for the excitation at 10 and 20 Hz.

V. CONCLUSION

A semiactive fuzzy controller using a squeeze-mode MR damper is presented for the structure's vibration reduction. To investigate modeling of the squeeze-mode MR damper for the fuzzy controller design, the Bouc–Wen model is used to describe the dynamics of the nonlinear force–displacement relation first. Because using the Bouc–Wen model to characterize the squeeze-mode MR damper needs a lookup table of system parameters for the application with various amplitudes and frequencies, a biviscosity model is proposed to describe the MR damper. This model is more robust for the various excitations with different amplitudes or frequencies than the Bouc–Wen model. To evaluate the parameters of the nonlinear MR damper and the cantilever shaft, GA optimization is used. For the proposed semiactive fuzzy controller, the fuzzy rules are determined using the GA optimization based on the windowed RMS acceleration. To establish the consistency of the simulation and real-time experimental results, the proposed fuzzy controller was implemented in real time using the NI CompactRIO in two case studies. The experimental results thus verified the effectiveness of the proposed controller and the consistency with the simulation results. To improve the performance of the fuzzy controller, novel self-tuning active control laws were proposed for this MRF damper as the excitation's frequency is low. Resulting from Fig. 13, the proposed controller has the better vibration reduction (13.4%) than the one of the fuzzy control in Case I (2.83%). Therefore, the self-tuning method shows the improvement for small amplitudes at low frequency. The proposed self-tuning controller has an almost 27% reduction in amplitude for the frequencies which are changed from 10 to 20 Hz.

REFERENCES

[1] A. G. Olabi and A. Grunwald, "Design and application of magneto-rheological fluid," *Mater. Design*, vol. 28, pp. 2658–2664, 2007.
[2] R. W. Phillips, "Engineering applications of fluids with a variable yield stress," Ph.D dissertation, Univ. California, Berkeley, CA, USA, 1969.
[3] K. C. Schuter and P. N. Roschke, "Fuzzy modeling of a magnetorheological damper using ANFIS," in *Proc. 9th IEEE Int. Conf. Fuzzy Syst.*, 2000, vol. 1, pp. 122–127.
[4] J. D. Carlson, D. M. Catanzarite, and K. A. St. Clair, "Commercial magneto-rheological fluid device," in *Proc. 5th Int. Conf. ER Fluids, MR Fluids Associated Technol.*, 1995, pp. 20–28.
[5] S. F. Dong, K. Q. Lu, J. Q. Sun, and K. Rudolph, "Adaptive force regulation of muscle strengthening rehabilitation device with magnetorheological fluids," *IEEE Trans. Neural Syst. Rehabil. Eng.*, vol. 14, no. 1, pp. 55–63, Mar. 2006.
[6] Q. Zhao and Y. X. Yang, "Improved single neuron PID control for heavy-duty vehicle magnetorheological seat suspension," in *Proc. IEEE Vehicle Power Propulsion Conf.*, Sep. 2008, pp. 1–3.
[7] R. Villamizar, N. S. Luo, S. J. Dyke, and J. Vehi, "Experimental verification of a backstepping controller for magnetorheological dampers in structural control," in *Proc. IEEE Int. Symp. Intell. Control, Mediterrean Conf. Control Autom.*, Jun. 27–29, 2005, pp. 316–321.
[8] P. Y. Lin, P. Roschke, and C. H. Loh, "System identification and real application of the smart magneto-rheological damper," in *Proc. IEEE Int. Symp. Intell. Control, Mediterrean Conf. Control Autom.*, Jun. 27–29, 2005, pp. 989–994.
[9] X. C. Zhu, X. J. Jing, and L. Cheng, "Magnetorheological fluid dampers: A review on structure design and analysis," *J. Intell. Mater. Syst. Struct.*, vol. 23, no. 8, pp. 839–873, May 2012.
[10] X. Z. Zhang, X. L. Gong, and P. Q. Zhang, "Study on the mechanism of the squeeze-strengthen effect in magnetorheological fluids," *J. Appl. Phys.*, vol. 96, no. 4, pp. 2359–2364, Aug. 2004.
[11] D. H. Wang and W. H. Liao, "Magnetorheological fluid dampers: A review of parametric modeling," *Smart Mater. Struct.*, vol. 20, no. 2, pp. 023001-1–023001-34, 2011.
[12] B. F. Spencer, Jr., S. J. Dyke, M. Sain, and J. D. Carlson, "Phenomenological model of a magnetorheological damper," *ASCE J. Eng. Mech.*, vol. 123, pp. 230–238, 1997.
[13] G. M. Kamath and N. Wereley, "Nonlinear viscoelatic-plastic mechanism-based model of an electro-rheological damper," *AIAA J. Guid., Control Dyn.*, vol. 20, no. 6, pp. 1125–1332, 1997.
[14] W. H. Li, G. Z. Yao, G. Chen, S. H. Yeo, and F. F. Yap, "Testing and steady state modeling of a linear MR damper under sinusoidal load," *J. Smart Mater. Struct.*, vol. 9, no. 1, pp. 95–102, 2000.

[15] C. C. Chang and P. Roschke, "Neural network modeling of a magnetorheological damper," *J. Intell. Mater. Syst. Struct.*, vol. 9, no. 9, pp. 755–764, 1998.
[16] C. C. Chang and P. Roschke, "Neural network emulation of inverse dynamics for a magnetorheological damper," *J. Struct. Eng.*, vol. 128, no. 2, pp. 231–239, 2002.
[17] K. C. Schurter and P. N. Roschke, "Fuzzy modeling of a magnetorheological damper using ANFIS," in *Proc. IEEE Int. Conf. Fuzzy Syst.*, 2000, pp. 122–127.
[18] G. Jin, M. K. Sain, K. D. Pham, B. F. Spencer, Jr., and J. C. Ramallo, "Modeling MR-dampers: A nonlinear blackbox approach," in *Proc. Amer. Control Conf.*, 2001, pp. 429–434.
[19] A. Leva and L. Piroddi, "NARX-based technique for the modelling of magneto-rheological damping devices," *Smart Mater. Struct.*, vol. 11, no. 1, pp. 79–88, 2002.
[20] G. Z. Yao, F. F. Yap, G. Chen, W. H. Li, and S. H. Yeo, "MR damper and its application for semi-active control of vehicle suspension system," *Mechatronics*, vol. 12, pp. 963–973, 2002.
[21] K. M. Choi, S. W. Cho, H. J. Jung, and I. W. Lee, "Semi-active fuzzy control for seismic response reduction using magnetorheological dampers," *Earthquake Eng. Struct. Dyn.*, vol. 33, pp. 723–736, 2004.
[22] H. Du, K. Y. Sze, and J. Lam, "Semi-active control of vehicle suspension with magneto-rheological dampers," *J. Sound Vib.*, vol. 283, pp. 981–996, 2005.
[23] M. Zapateiro, F. Pozo, H. R. Karimi, and N. Luo, "Semiactive control methodologies for suspension control with magnetorheological dampers," *IEEE/ASME Trans. Mechatronics*, vol. 17, no. 2, pp. 370–380, Apr. 2012.
[24] S. B. Choi, S. K. Lee, and Y. P. Park, "A hysteresis model for the field-dependent damping force of a magnetorheological damper," *J. Sound Vib.*, vol. 245, no. 2, pp. 375–383, 2001.
[25] L. Alvarez and R. Jimenez, "Real-time identification of magneto-rheological dampers," in *Proc. 15th IFAC*, 2002, p. 1583-1583.
[26] L. A. Zadeh, "Fuzzy set," *Inf. Control*, vol. 8, pp. 338–353, 1965.
[27] E. H. Mamdani, "Application of fuzzy algorithm for control of simple dynamic plants," *Proc. Inst. Elect. Eng.*, vol. 121, pp. 1585–1588, 1974.
[28] M. Battaini, F. Casciati, and L. Faravelli, "Fuzzy control of structural vibration: An active mass system driven by a fuzzy controller," *Earthquake Eng. Struct. Dyn.*, vol. 27, pp. 1267–1276, 1998.
[29] T. L. Teng, C. P. Peng, and C. Chuang, "A study on the application of fuzzy theory to structural active control," *Comput. Methods Appl. Mech. Eng.*, vol. 189, pp. 439–448, 2000.
[30] A. P. Wang and C. D. Lee, "Fuzzy sliding mode control for a building structure based on genetic algorithms," *Earthquake Eng. Struct. Dyn.*, vol. 31, pp. 881–895, 2002.
[31] C. J. Lin, H. T. Yau, and Y. C. Tian, "Identification and compensation of nonlinear friction characteristics and precision control for a linear motor stage," *IEEE/ASME Trans. Mechatronics*, vol. 18, no. 4, pp. 1385–1396, Aug. 2013.
[32] Corporation Lord, *MRF-122EG Magneto-Rheological Fluid*. (2013). [Online]. Available: http://www.lord.com/products-and-solutions/magneto-rheological-(mr)/product.xml/1644/1
[33] J. L. Sproston, S. G. Rigby, E. W. Williams, and R. Stanway, "A numerical simulation of electrorheological fluids in oscillatory compressive squeeze-flow," *J. Phys. D, Appl. Phys.*, vol. 27, pp. 338–342, 1994.
[34] S. J. Dyke, B. F. Spencer, M. K. Sain, and J. D. Carlson, "Modeling and control of magnetorheological dampers for seismic response reduction," *Smart Mater. Struct.*, vol. 5, pp. 565–575, 1996.
[35] J. C. Dixon, *The Shock Absorber Handbook*, SAE International, Troy, MI, USA, 1999.

Chih-Jer Lin (M'12) received the B.S., M.S., and Ph.D. degrees from National Cheng Kung University, Tainan, Taiwan, in 1992, 1994, and 1998, respectively, all in mechanical engineering.

He is currently a Professor in the Graduate Institute of Automation and Technology, National Taipei University of Technology, Taipei, Taiwan. His current research interests include mechatronics, vibration control, motion control, system identification, sliding-mode control, robotics, and evolutionary algorithms.

Her-Terng Yau (M'11) received the B.S. degree from National Chung Hsing University, Taichung, Taiwan, in 1994, and the M.S. and Ph.D. degrees from National Cheng Kung University, Tainan, Taiwan, in 1996 and 2000, respectively, all in mechanical engineering.

He is currently a Professor in the Department of Electrical Engineering, National Chin-Yi University of Technology, Taichung, Taiwan. His current research interests include energy converter control, system control of mechatronics, and nonlinear system analysis and control.

Chun-Ying Lee received the Graduate degree from the Department of Mechanical Engineering, National Taipei Institute of Technology, Taipei, Taiwan, in 1980, the M.S. degree in mechanical engineering from National Sun Yat-sen University, Kaohsiung, Taiwan, in 1985, and the Ph.D. degree in engineering mechanics from Michigan State University, East Lansing, MI, USA, in 1991.

He is currently a Professor in the Department of Mechanical Engineering, National Taipei University of Technology, Taipei. His current research interests include smart materials, vibration control, and supercritical carbon-dioxide-assisted electroplating process.

Kai-Hung Tung received the B.S. degree from National Yunlin University of Technology, Yunlin, Taiwan, in 2010, and the M.S. degree from National Taipei University of Technology, Taipei, Taiwan, in 2012, in automation technology.

He is currently fulfilling mandatory military service. His research interests include system identification of mechatronics, vibration control, MRF, and nonlinear system analysis.